

# Recrystallization Behavior and Super-Elasticity of a Metastable $\beta$ -Type Ti-21Nb-7Mo-4Sn Alloy During Cold Rolling and Annealing

Siyao Lu, Fengcang Ma, Ping Liu, Wei Li, Xinkuan Liu, Xiaohong Chen, Ke Zhang, Qingyou Han, and Lai-Chang Zhang

(Submitted November 27, 2017; in revised form March 26, 2018; published online July 2, 2018)

Based on the d-electron alloy design theory, a new metastable  $\beta$ -type titanium alloy for biomedical applications, Ti-21Nb-7Mo-4Sn (wt.%) was designed in this article. This theory predicted this alloy was a metastable single  $\beta$ -type titanium alloy with low elastic modulus at room temperature, and the  $\beta$ -phase transition ( $\beta$  to  $\alpha'$ ) would be easy to occur during the cold rolling. The evolution of microstructure and mechanical properties of this alloy during cold rolling plus annealing were investigated by means of x-ray diffraction, optical microscope, transmission electron microscope and mechanical properties test. The results indicate that only  $\beta$  phase can be identified in this alloy before cold rolling, while a large amount of lath martensite ( $\alpha''$  phase) appears after cold rolling due to stress-induced martensitic transformation, which is in accordance with the prediction of the d-electron alloy design theory. The recrystallization nucleation occurs preferentially in the martensite lath region during the subsequent annealing process, and this region forms a large number of nano-crystals and microcrystals, showing that cold rolling plus annealing can become a new process for refining grains. Compared with casting and cold rolling samples, the annealing materials at 923 K for 10 min have excellent comprehensive mechanical properties with lower elastic modulus (58 GPa) and higher elastic recovery rate (35.39%).

**Keywords** low Young's modulus, mechanical property, microstructure evolution, super-elasticity, titanium alloys

## 1. Introduction

Titanium and titanium alloys have been widely used for medical materials for years due to their light weight, excellent mechanical properties, outstanding biocompatibility and primary resistance to corrosion (Ref 1, 2). The demand for titanium and titanium alloys is increasing rapidly because of the growing population of elderly person, who are in higher danger of bone-tissue damage. To date, Ti-Ni alloys have been used for a large number of medical materials for years, but their Young's modulus is higher than human skeleton, which will cause the stress-shielding effect (Ref 3-5). Also, new types of Nickel-free titanium alloys, adding innocuous elements such as Nb, Mo and Sn to obtain the low elastic modulus and high strength, have been highly applied because of the cytotoxicity and Ni-hypersensitivity of nickel products (Ref 6-9).

Previous investigations show that the metastable  $\beta$ -type Ti alloys have a large amount of phase transformations, including

$\beta$ -phase with body-centered cubic structure,  $\alpha$  phase with hexagonal close-packed structure,  $\alpha'$  phase with hexagonal close-packed structure,  $\alpha''$  phase with orthorhombic structure and  $\omega$  phase with hexagonal structure (Ref 10-12). It is generally known that the low Young's modulus and super-elastic behavior of  $\beta$ -type titanium alloys are owing to the reversible martensitic transformation between  $\alpha''$  phase and parent phase (Ref 13, 14). The martensitic transformation temperature ( $M_s$ ) and the mechanical properties of Ti alloys depend on their compositions (Ref 15).

A new approach for alloy design which is based on the molecular orbital calculation of electronic structures has been put forward recently. The compositions of those  $\beta$ -type titanium alloys, such as Ti-Nb, Ti-Ta and Ti-Zr, have been developed. Tane et al. (Ref 5) found the  $M_s$  of Ti-Nb alloys descend to  $-90^\circ\text{C}$  with the increase in the Nb content. The super-elasticity strain can be improved, but other performance cannot be improved because of their low martensitic transformation stress with the addition of Nb. Tahara et al. reported (Ref 7) most of the metastable  $\beta$ -type Ti alloys are ternary or quaternary alloys, making it difficult to get homogeneous structure. In order to get excellent properties, Sn are checked as auxiliary elements, with the  $\beta$ -stabilizers (i.e., Nb, Mo). Al-Zain (Ref 8) investigated that Ti-Mo alloys possess a smaller super-elasticity strain, but a high martensitic transformation stress. In addition, previous investigations have shown that that  $M_s$  was declining sharply with the increase in Sn element, and then, a large super-elasticity strain was obtained.

In this work, the microstructures were observed and super-elasticity and elastic modulus were measured after cold rolling and annealing treatment, and the effect of cold rolling and annealing temperature on martensitic transformation and mechanical properties was studied.

Siyao Lu, Fengcang Ma, Ping Liu, Wei Li, Xinkuan Liu, Xiaohong Chen, and Ke Zhang, School of Materials Science and Engineering, University of Shanghai for science and technology, Shanghai 200093, China; and Qingyou Han, Department of Mechanical Engineering Technology, Purdue University, West Lafayette, IN 47907, USA; and and Lai-Chang Zhang, School of Engineering, Edith Cowan University, 270 Joondalup Drive, Joondalup, Perth, WA 6027, Australia. Contact e-mails: mafengcang@163.com, mafengcang@usst.edu.cn.

## 2. Experimental Procedures

### 2.1 Alloy Design

According to Morinaga's study (Ref 16), a new way for alloy design which was based on the molecular orbital calculation of electronic structures has been presented. The electronic structure of titanium alloy has been calculated by molecular orbital method, and two alloying parameters ( $\overline{Bo}$  and  $\overline{Md}$ ) were theoretically determined.  $\overline{Bo}$  (the bond order) is served to characterize the overlap of electron clouds between atoms and measure the covalent bond strength between atoms, and  $\overline{Md}$  (the metal d-orbital energy level) is used to define the combined effects of atomic size, electronegativity and alloying. For multicomponent alloys, the value of  $\overline{Md}$  and  $\overline{Bo}$  calculated as the alloy composition is defined as (Ref 17, 18)

$$\overline{Md} = \sum_i^n X_i(\overline{Md})_i \quad (\text{Eq 1})$$

$$\overline{Bo} = \sum_i^n X_i(\overline{Bo})_i \quad (\text{Eq 2})$$

where  $X_i$ ,  $(\overline{Md})_i$  and  $(\overline{Bo})_i$  are the atomic percentage, and the value of  $\overline{Md}$  and  $\overline{Bo}$  of alloying element  $i$ , respectively.

The  $\overline{Md}$  and  $\overline{Bo}$  values of the different elements (Ti, Nb, Mo, Sn) in the titanium alloy are shown in Table 1.

The boundaries of single phase ( $\alpha$ ,  $\beta$ ) and multiphase mixing regions ( $\alpha + \beta$ ) together with the boundaries for  $M_s$  and  $M_f$  (room temperature) are indicated in Fig. 1. Abdel-Hady (Ref 17) discovered the distribution of elastic modulus follows a certain rule in  $\overline{Bo}$ - $\overline{Md}$  diagram: The closer the transition line, the lower the elastic modulus, and the elastic modulus decreases with the increase in  $\overline{Bo}$  and  $\overline{Md}$  values. So as to get the low elastic modulus of the alloy, in the guarantee conditions for  $\beta$ -type alloys, alloy designed in this paper should have high  $\overline{Bo}$  and  $\overline{Md}$  values. For our alloy, Ti-21Nb-7Mo-4Sn (wt.%), the values of  $\overline{Md}$  and  $\overline{Bo}$  are calculated to be 2.831 and 2.417, respectively, which is located between boundaries for the single phase ( $\alpha$ ,  $\beta$ ) and multiphase mixing region phases ( $\alpha + \beta$ ) and close to the boundary for  $M_s$  (indicated by a pentagon in the map), showing that it is probably that this material is a metastable  $\beta$ -type titanium alloy with low elastic modulus for biomedical applications.

### 2.2 Alloy Preparation and Characterization

In this paper, Ti-21Nb-7Mo-4Sn (wt.%) alloy ingot was manufactured by arc recasting with titanium particles

**Table 1** The value of  $\overline{Bo}$  and  $\overline{Md}$  of different elements (Ti, Nb, Mo, Sn) and material composition in this study (Ref 17)

Elements	$(\overline{Bo})_i(\text{hcp})/(\overline{Bo})_i(\text{bcc})$	$(\overline{Md})_i/\text{eV}$	Composition (wt.%)
3d			
Ti	3.513/2.790	2.447	68
4d			
Nb	3.767/3.099	2.424	21
Mo	3.759/3.063	1.961	7
5d			
Sn	2.782/2.283	2.100	4

(99.995%), niobium particles (99.95%), molybdenum particles (99.95%), tin particles (99.95%). In order to ensure the homogenization of composition, the ingot was melted 5 times and homogenized at 1273 K for 6 h. After that cold rolling (CR) at 90%, and then annealing for 10 min at 823, 923, 1023 K, respectively, and subsequently cooling in the air ( $\sim 298$  K), these specimens were named as CRA specimens.

The samples were prepared with the conventional technique of grinding and mechanical polishing, etched by Kroll's reagent, and the microstructure was observed with optical microscope (OM). By an x-ray diffraction (XRD) machine, the lattice constants of the parent and martensitic phases were measured. The microstructures were explored by transmission electron microscopy (TEM), using a JEM-2010 electron microscope operated at 200 kV. The super-elastic behaviors of those samples were studied by nano-indentation (NANO Indenter G200). Under continuous conditions, the experiments were carried out by forcing the diamond Berkovich indenter into the specimens. In the whole indentation process, the displacement of the indenter was measured simultaneously with the controlled force (Ref 13). During the indentation cycle, the force increased to the maximum and then decreased to zero. The maximum load applied during the indentation test was 10 mN.

## 3. Results and Discussion

### 3.1 XRD Structure Determination

Figure 2(a) and (b) shows the XRD patterns of casting and cold rolling (CR) samples. Only diffraction peaks of  $\beta$ -phase can be identified from the patterns of the alloy in casting, while peaks of  $\alpha''$  phase appear after cold rolling. This indicates that  $M_s$  of this alloy is below room temperature, and the appearance of the martensite implies that the deformation induces the martensitic transformation ( $\beta$  to  $\alpha''$ ). The grain boundaries of the sample will be crushed with the increase in rolling

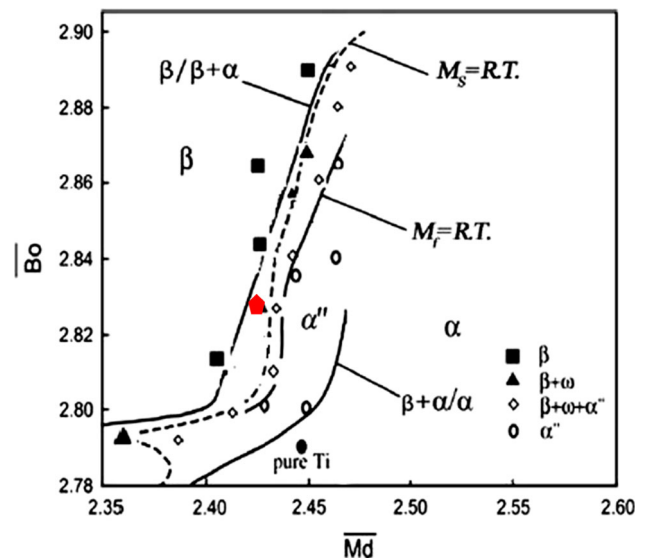


**Fig. 1**  $\overline{Md}$  and  $\overline{Bo}$  map in which the boundaries for the single phase ( $\alpha$ ,  $\beta$ ) and multiphase mixing region phases ( $\alpha + \beta$ ) are shown together with the boundaries for  $M_s$  and  $M_f$  (Ref 19)

deformation, and almost all of the grain boundaries are not complete and lattice distortion is serious at the deformation rate to 90%.

A few phase transformations took place under different annealing temperatures as shown in Fig. 2(c), (d) and (e). Compared with the rolling samples, the content of  $\alpha''$  phase decreases and the stability of  $\beta$  improves relatively with the increase in the annealing temperature. This indicates that an inverse phase transition ( $\beta$  to  $\alpha''$ ) occurs during the annealing process, and stress and dislocation caused by rolling also

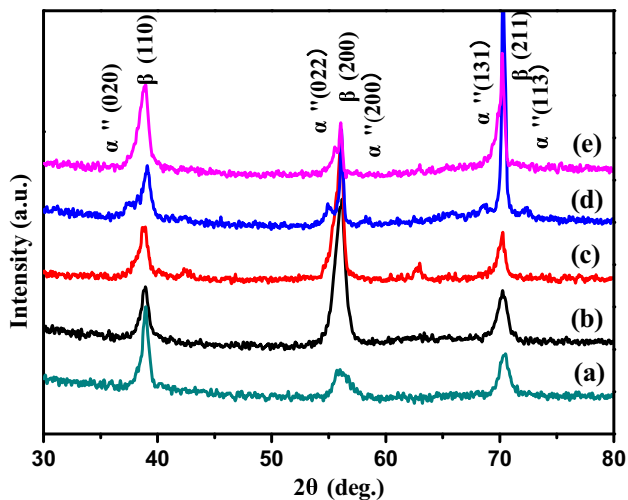


**Fig. 2** XRD patterns of the casting (a), cold rolling (b) and annealing at 823 K (c), 923 K (d), 1023 K (e) Ti-21Nb-7Mo-4Sn alloy

provide energy for this solid-phase evolution. The specific process of phase transformation is analyzed by OM (Fig. 3) and TEM (Fig. 5.)

### 3.2 Microstructure Evolution

**3.2.1 Metallographic Analysis.** After rolling deformation (90%), the grain boundaries are pulled into a strip along the rolling directions which can be vaguely seen in Fig. 3(a), and it can be apparently observed that parallel acicular and fine  $\alpha''$  phase appears near the prior  $\beta$ -grain boundary. These results show that the crystal boundary of the alloy is not clear by cold rolling which confirms previous conjecture in Fig. 2, and the internal stress produced by cold rolling leads to the occurrence of stress-induced martensite transformation. The phase transition occurs preferentially at the original grain boundaries because of the higher energy and internal stress.

With different annealing temperatures, the microstructures of the samples are shown in Fig. 3(b), (c) and (d). Specific mechanisms need further investigation. The  $\alpha''$  phase and recrystallized grains can be clearly seen in Fig. 3(b), due to the elimination of stress and the occurrence of recrystallization during annealing. The recrystallized grains are preferentially present in the original grain boundary region and the prior lath martensitic area because the dislocation at the grain boundary and the accumulation of stress provide the required energy for the recrystallization nucleation. The recrystallized grains existing in the original lath martensitic region can be clearly seen in Fig. 3(c), while the regions without martensitic transformation have not yet begun recrystallization. In Fig. 3(d), the samples have been completely recrystallized, and the grains growing preferentially in the recrystallized region have grown. The

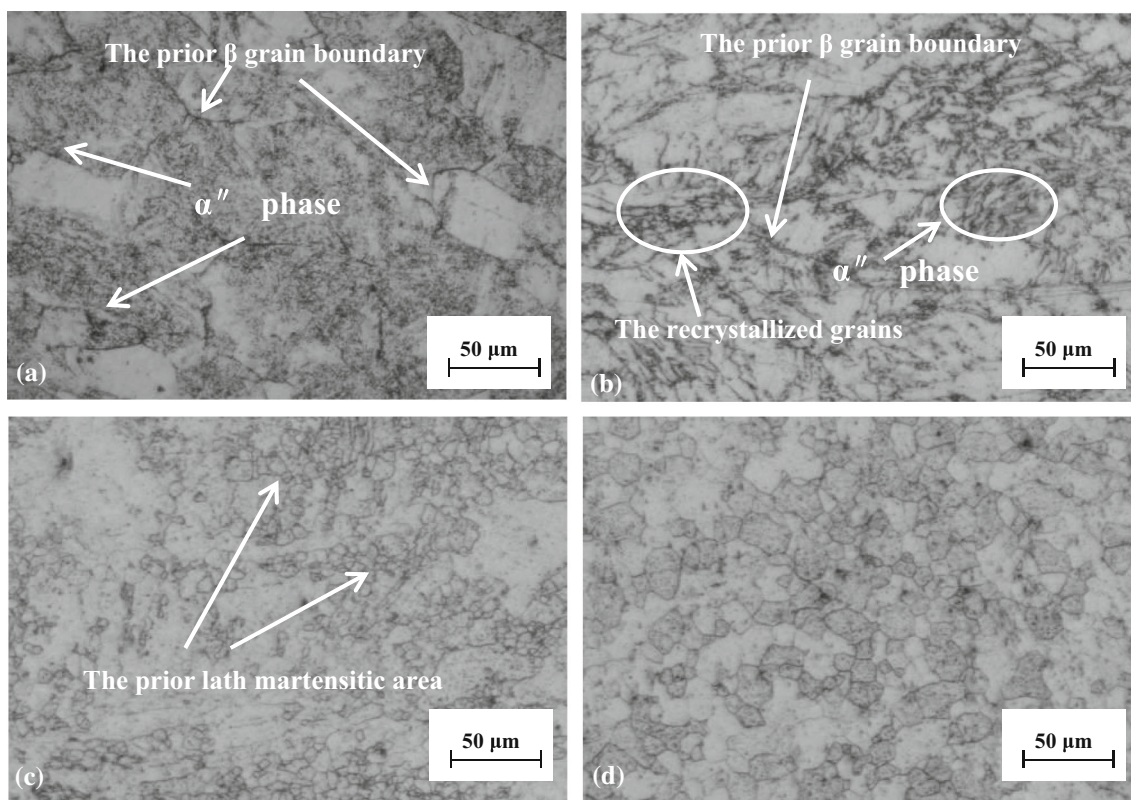


**Fig. 3** Optical micrographs of the CR (a) and CRA at 823 K (b), 923 K (c), 1023 K (d) Ti-21Nb-7Mo-4Sn alloy



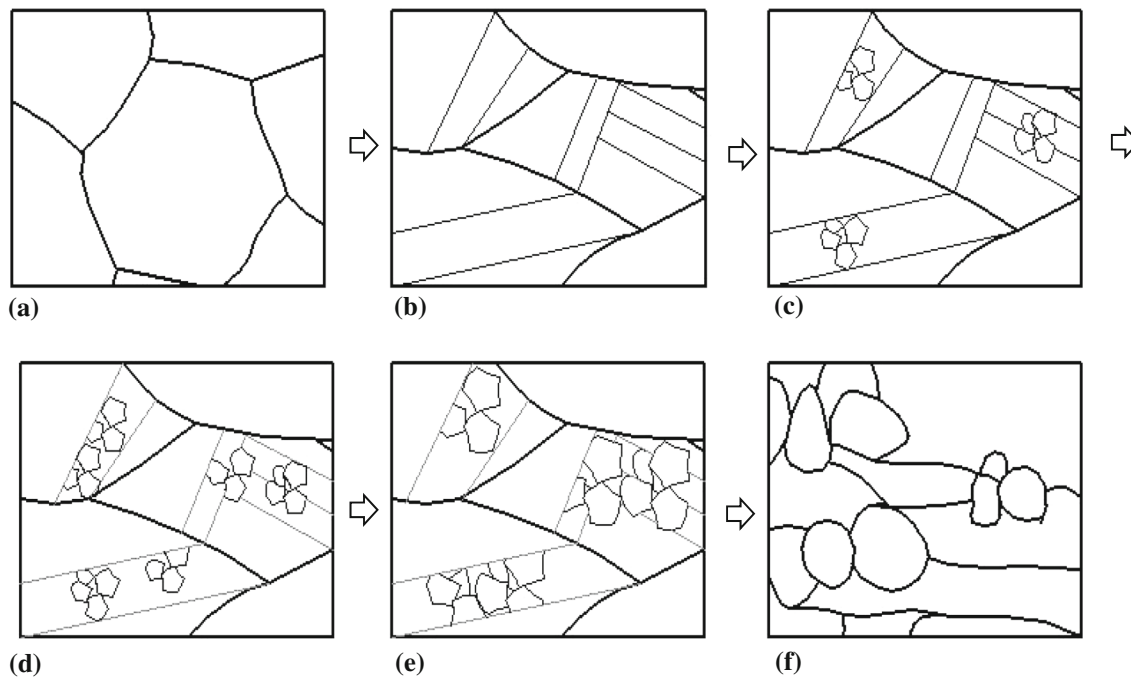


**Fig. 4** Schematic diagram of microstructure evolution of the CRA Ti-21Nb-7Mo-4Sn alloy

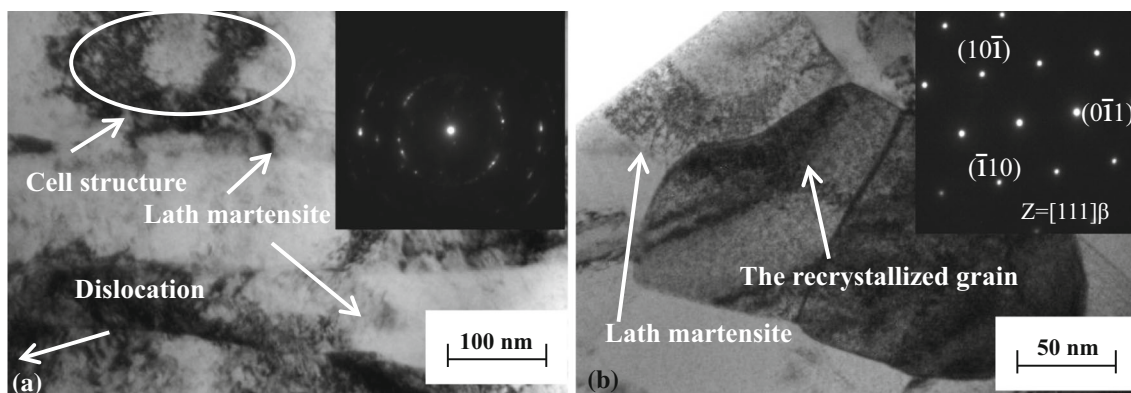


**Fig. 5** The TEM micrographs of the cold rolling by 90% (a) and cold rolling plus annealing at 923 K for 10 min (b) specimens

reasons for these changes can be explained: (a) High temperature can eliminate the rolling grain boundary and grain is not clear, so in the annealing diagram we can clearly see the martensitic phase. The increase in temperature causes the recrystallization nucleation and growth time to be shortened due to the acceleration of atomic thermal motion. (b) The nucleation takes precedence over the martensitic transformation zone in the rolling, since the dislocations and internal stresses present here can provide the energy required for recrystallization.

Schematic diagram of microstructure evolution of the CRA alloy is shown in Fig. 4. The cast microstructure is shown in Fig. 4(a). With the rolling deformation (at 90%), the grain boundaries are elongated and blurred, accompanied by the presence of martensitic lath, as shown in Fig. 4(b). Figure 4(c), (d), (e) and (f) describes the process of the sample's microstructure during annealing. With the increase in deformation amount, the lath martensitic number increases, and after annealing, fine grain is formed on martensitic lath. The formation of crystallites

indicates that there is also some lattice rotation within the martensitic lath to fit the strain of the region and the surrounding area. As the temperature varies, the number of sliding systems in the deformation band is different, resulting in the rotation of the lattice not uniform and synchronous, and they gradually evolve into fine grain with large angle grain boundaries. Due to uneven deformation, which evolved into the fine grains are also more obvious at the grain boundary. Recrystallization nucleation occurs on martensite lath, and the grain grows up with the increase in temperature. These recrystallized grains are  $\beta$ -phase, which can be confirmed in Fig. 5(b). Therefore, the formation of nano-structures is closely related to the evolution of martensitic lath. Due to the large shear strain in the slab, it is necessary to adjust and adapt to the elastic strain by lattice rotation. With the increase in the amount of macroscopic plastic deformation, the tangent strain of the deformation zone increases, resulting in an increase in the lattice rotation, and the angle of the lattice rotation increases, and the volume fraction of the microcrystals and nanocrystals increases and the size decreases. With regard to the

formation of nano-crystals, it is generally believed that in the alloy, martensitic transformation, twins, kinks, deformation bands, giant defects, etc., caused structural instability and the interaction between them to break the crystal. The process of phase transition is fully demonstrated in Fig. 6, including stress-induced martensitic transformation and its inverse phase transition.

**3.2.2 Transmission Electron Microscopy (TEM) Analysis.** The TEM micrograph of the cold rolling is shown in Fig. 5(a). It is clear that lath martensite and dislocation areas have been marked with arrows, respectively. A lot of lath martensite can be seen in the direction of rolling. In dislocation region, more dislocation tangles and dislocation loops can be observed and even formed a small cell structure. With the cold rolling process, the lath martensite is divided into several thin lamellae by dislocation, which can lead to grain refinement. A small amount of deformation and twin martensitic phase were observed. This is why the larger deformation causes the lattice to be distorted. Martensitic transformation is related to grain size, grain refinement inhibits martensitic transformation (Ref 20). In addition, dislocation entanglements in deformed microstructures of cold-rolled alloys may hinder martensitic transformation, and the internal stress caused by cold rolling leads to the emergence of a sea of dislocations and the martensitic transformation. The results show that the sample with a reduction rate of 90% has great influence on dislocations and lath martensite. Thus, diffraction rings are formed, as shown in the upper right corner of Fig. 5(a).

As shown in Fig. 5(b), the recrystallized grains can be observed in the annealed samples, which are formed on lath martensite, and the selected electron diffraction pattern corresponding to the recrystallized grains is shown in the upper right corner. Recrystallized grains are formed in the martensite and dislocation entanglements regions, which provide the energy required for nucleation. In addition, the recrystallized grains of nano-crystalline can be observed in annealed samples, and the recrystallization is completely controlled and the grain growth is restrained due to the short annealing time and suitable temperature. In many metastable  $\beta$ -type titanium alloys, it is easy to induce martensitic transformation and grain refinement (Ref 21). It is found that the martensitic transformation and the reverse transformation of  $\alpha''$  martensite play an important role in grain refinement (Ref 22).

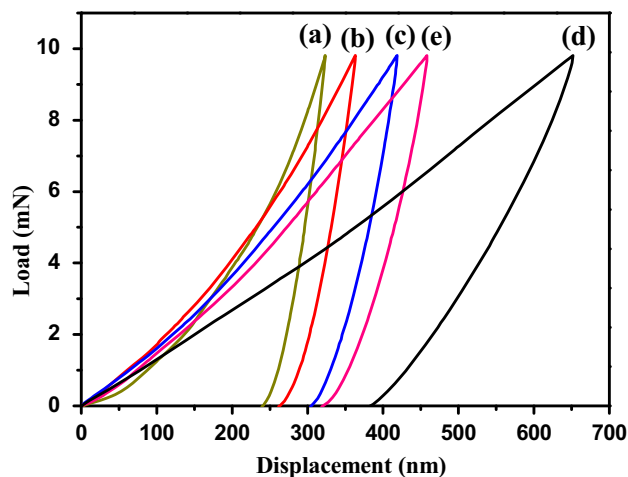


**Fig. 6** Nano-indentation load–displacement curves of the casting (a), cold rolling (b) and annealing at 823 K (c), 923 K (d), 1023 K (e) Ti-21Nb-7Mo-4Sn alloy

The experimental results of this alloy, XRD and TEM show that the Ti-21Nb-7Mo-4Sn alloy exhibits a metastable  $\beta$ -phase on the martensitic transformation. Thus, it can be concluded that the reason for grain refinement in annealed specimens is the stress-induced martensitic transformation during cold rolling and the reverse transformation of martensite during annealing. Previous studies have shown that microstructures greatly affect martensitic transformation (Ref 23). Based on the above observation results, it can be concluded that the grain refinement, dislocation density and nanometer martensite play an important role in the martensitic transformation of annealed samples.

### 3.3 Mechanical Properties

Load–displacement tests were carried out at 8 different locations on the specimen surface. The average value is then calculated to determine the super-elastic behavior of the samples. A representative set of nano-indentation load–displacement curves with 10 mN are shown in Fig. 6. Under the same load, as the annealing temperature increases, the indentation depth of the indenter increases gradually. This indicates that rolling leads to severe deformation of the material, resulting in a large number of dislocations within the material. These dislocations are tangled to each other, and some form a dislocation ring, which increase the hardness of the material. With the increase in annealing temperature, the internal stress of the specimen disappears, and recrystallization occurs gradually in the dislocation region, which lead to material resistance to external deformation capacity weakened.

The load–displacement curve of materials can be measured by nano-indentation. The deformation mechanism of materials with different crystal structures leads to different load–displacement curves. Since the nano-indentation has high load–displacement resolution, the load–displacement curve can reflect whether the material has undergone a solid-state phase transition during the indenter indentation, especially the pressure dependent solid-state phase transition. Stress-induced martensitic transformation is a kind of solid phase process. If the the parent phase is applied force at temperature above  $M_s$ , the mechanical energy serving the driving force of the matensite transformation, this transformation may occur even at the temperature above  $M_s$  (Ref 24, 25). Since the volume of martensite is greater than the specific volume of the parent phase, the superplasticity of the material occurs during the transformation. When the external force is eliminated, the martensite reverses into a parent phase, and the macroscopic performance of the material is elastic recovery. Based on the above principle, the total and recovered work ( $W_t$ ,  $W_{rc}$ ) and the elastic recovery rate ( $\eta$ ) can be calculated (Ref 26, 27):

$$W_t = \int_0^{D_{max}} L_1 dD \quad (\text{Eq 3})$$

$$W_{rc} = \int_{D_r}^{D_{max}} L_2 dD \quad (\text{Eq 4})$$

$$\eta = \frac{W_{rc}}{W_t} \quad (\text{Eq 5})$$

where  $D_{max}$  is the maximum indentation depth of the press head,  $D_r$  is the indentation depth after unloading,  $L_1$  is the loading force, and  $L_2$  is the unloading force.

The elastic modulus measured directly by nano-indentation and elastic recovery rate calculated by formulas (3), (4) and (5)

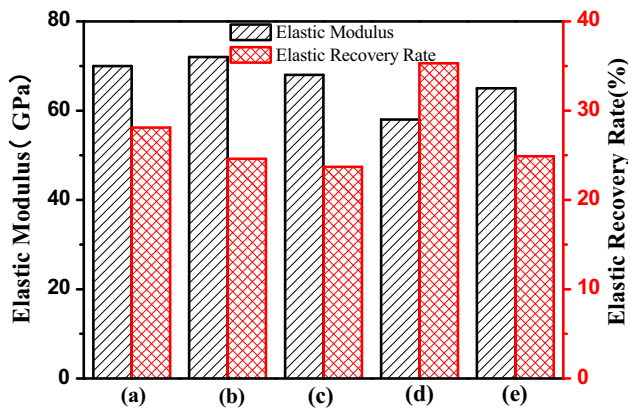


**Fig. 7** Elastic modulus and elastic recovery rate of the casting (a), cold rolling (b) and annealing at 823 K (c), 923 K (d), 1023 K (e) Ti-21Nb-7Mo-4Sn alloy

of the samples in different processing states are shown in Fig. 7. It can be found that the elastic modulus of this material under these different processing methods is about 65 GPa. The effect of the cold rolling on Young's modulus is not obvious, but the effect at different annealing temperatures is significant: The elastic modulus of cold rolling (72 GPa) is slightly higher than that of the casting (70 GPa), but the annealing states are lower than the cold rolling and the casting's, and it can be seen that the overall trend of the annealing elastic modulus is decreased first and then increased and reaches a minimum (58 GPa) at 923 K. As shown in Fig. 5, the stress caused by cold rolling promotes martensitic transformation ( $\beta$  to  $\alpha''$ ) and the inverse phase transformation ( $\alpha''$  to  $\beta$ ) occurs during recrystallization annealing, or the large number of dislocations and internal stresses produced by rolling are eliminated during the annealing process, leading to these phenomena.

The change in elastic recovery rate is opposite to the elastic modulus in the above process. The recovery rate of cold rolling (24.61%) is lower than that of casting (28.09%) because of the existence of over-dislocation and martensitic lath, the unclear grain boundary and the crystal structure close to the amorphous. The elastic recovery mainly depends on the phase transformation ( $\beta$  to  $\alpha''$ ) and inverse phase transformation of the material ( $\alpha''$  to  $\beta$ ): stress-induced martensitic transformation in the sample during loading and the reverse transformation during unloading. In the annealing stage, the elastic recovery increased firstly, reaching the maximum at 923 K (35.39%), and then decreased. Recrystallization annealing makes the fine grain of the  $\beta$ -phase form on the martensite, increases the content of the  $\beta$ -phase and provides the condition for the stress-induced martensite transformation during the loading (Ref 28). The reduction of the grain size led to the increase in the volume ratio of grain boundaries and voids (Ref 29). Therefore, the elimination of material dislocation and internal stress, recrystallization, and high content of  $\beta$ -phase make the sample obtain better comprehensive properties ( $E$ (58 GPa),  $\eta$ (35.39%)).

## 4. Conclusions

In the present work, the evolution of microstructure and mechanical properties of the Ti-21Nb-7Mo-4Sn alloy were investigated and the following conclusions have been reached:

1. This alloy can be only observed the  $\beta$ -phase before deformation, while a large amount of lath martensite ( $\alpha''$  phase) appears during cold rolling due to stress-induced martensitic transformation, indicating that the material is a metastable titanium alloy, which is in accordance with the result of the d-electron alloy design method. The phenomenon that annealing recrystallized grains preferentially nucleate on the lath martensite formed after rolling indicates that cold rolling plus annealing can become a new process for refining grains.
2. The elastic modulus of CRA sample annealing at 923 K for 10 min is 58 GPa, the casting is 70 GPa, and that of the CR sample is 72 GPa. The modulus of annealing sample is lowest, which may be attributed to the improvement of  $\beta$ -phase stability, the refinement of grains and the disappearance of dislocation and internal stress after annealing.
3. The elastic recovery rates of casting and CR samples are 24.61 and 28.09%, respectively, while that of the CRA samples annealing at 923 K is 35.39%. The reason for the highest elastic recovery rate of samples annealing at 923 K may be that a large number of defects and residual stress of casting and rolling materials can be eliminated by annealing, which is conducive to the subsequent stress-induced martensitic transformation and its reverse transformation. In addition, the appropriate annealing temperature and shorter annealing time can ensure the completion of recrystallization and the formation of microcrystalline and nano-crystalline.

## Acknowledgments

The authors acknowledge financial support provided by National Natural Science Foundation of China (Grant No. 51771119), Natural Science Foundation of Shanghai (Grant No. 17ZR1419600) and Scientific and Technological Key Project of Shanghai (Grant Nos. 11441900500 and 11441900501).

## References

1. Y.J. Liu, S.J. Li, H.L. Wang, W.T. Hou, Y.L. Hao, R. Yang, T.B. Sercombe, and L.C. Zhang, Microstructure, Defects and Mechanical Behavior of Beta-Type Titanium Porous Structures Manufactured by Electron Beam Melting and Selective Laser Melting, *Acta Mater.*, 2016, **113**, p 56–67
2. L.S. Wei, H.Y. Kim, and S. Miyazaki, Effects of Oxygen Concentration and Phase Stability on Nano-Domain Structure and Thermal Expansion Behavior of Ti-Nb-Zr-Ta-O Alloys, *Acta Mater.*, 2015, **100**(3), p 313–322
3. P. Barriobero-Vila, G. Requena, F. Warchomicka, A. Stark, N. Schell, and T. Buslaps, Phase Transformation Kinetics During Continuous Heating of a  $\beta$ -Quenched Ti-10 V-2Fe-3Al Alloy, *J. Mater. Sci.*, 2015, **50**(3), p 1412–1426
4. S. Ehtemam-Haghighi, K.G. Prashanth, H. Attar, A.K. Chaubey, G.H. Cao, and L.C. Zhang, Evaluation of Mechanical and Wear Properties of Ti-xNb-7Fe Alloys Designed for Biomedical Applications, *Mater. Des.*, 2016, **113**, p 592–599
5. M. Tane, K. Hagihara, M. Ueda, T. Nakano, and Y. Okuda, Elastic-Modulus Enhancement During Room-Temperature Aging and Its Suppression in Metastable Ti-Nb-Based Alloys with Low Body-Centered Cubic Phase Stability, *Acta Mater.*, 2016, **102**, p 373–384
6. E. Acar, H. Tobe, I. Kaya, H. Karaca, and Y. Chumlyakov, Compressive Response of  $Ni_{45.3}Ti_{34.7}Hf_{15}Pd_5$  and  $Ni_{45.3}Ti_{29.7}Hf_{20}Pd_5$  Shape-Memory Alloys, *J. Mater. Sci.*, 2015, **50**(4), p 1924–1934

7. M. Tahara, H.Y. Kim, T. Inamura, H. Hosoda, and S. Miyazaki, Lattice Modulation and Superelasticity in Oxygen-Added  $\beta$ -Ti Alloys, *Acta Mater.*, 2011, **59**(16), p 6208–6218
8. Y. Al-Zain, Y. Sato, H.Y. Kim, H. Hosoda, T.H. Nam, and S. Miyazaki, Room Temperature Aging Behavior of Ti-Nb-Mo-Based Superelastic Alloys, *Acta Mater.*, 2012, **60**(5), p 2437–2447
9. S. Ehtemam-Haghighi, G.H. Cao, and L.C. Zhang, Nanoindentation Study of Mechanical Properties of Ti Based Alloys with Fe and Ta Additions, *J. Alloy. Compd.*, 2017, **692**, p 892–897
10. L.Q. Wang, L.C. Xie, Y.T. Lv, L.C. Zhang, L.Y. Chen, Q. Meng, J. Qu, D. Zhang, and W.J. Lu, Microstructure Evolution and Superelastic Behavior in Ti-35Nb-2Ta-3Zr Alloy Processed by Friction Stir Processing, *Acta Mater.*, 2017, **131**, p 499–510
11. L.Q. Wang, W.J. Lu, J.N. Qin, F. Zhang, and D. Zhang, Texture and Superelastic Behavior of Cold-Rolled TiNbTaZr Alloy, *Mater. Sci. Eng., A*, 2008, **491**(1), p 372–377
12. Y.J. Liu, H.L. Wang, S.J. Li, S.G. Wang, W.J. Wang, W.T. Hou, Y.L. Hao, R. Yang, and L.C. Zhang, Compressive and Fatigue Behavior of Beta-Type Titanium Porous Structures Fabricated by Electron Beam Melting, *Acta Mater.*, 2017, **126**, p 58–66
13. L.Q. Wang, W.J. Lu, J.N. Qin, F. Zhang, and D. Zhang, Influence of Cold Deformation on Martensite Transformation and Mechanical Properties of Ti-Nb-Ta-Zr Alloy, *J. Alloy. Compd.*, 2009, **469**(1–2), p 512–518
14. H.Y. Kim, Y. Ikehara, J.I. Kim, H. Hosoda, and S. Miyazaki, Martensitic Transformation, Shape Memory Effect and Superelasticity of Ti-Nb Binary Alloys, *Acta Mater.*, 2006, **54**(9), p 2419–2429
15. Q.Q. Wei, L.Q. Wang, Y.F. Fu, J. Qin, W. Lu, and D. Zhang, Influence of Oxygen Content on Microstructure and Mechanical Properties of Ti-Nb-Ta-Zr Alloy, *Mater. Des.*, 2011, **32**(5), p 2934–2939
16. M. Morinaga, M. Kato, T. Kamimura, M. Fukumotom, I. Harada, K. Kubo, Theoretical design of b-type titanium alloys, in *Titanium 1992, Science and Technology, Proceedings of the Seventh International Conference on Titanium, San Diego, CA* (1992), pp. 276–83
17. M. Abdel-Hady, K. Hinoshita, and M. Morinaga, General Approach to Phase Stability and Elastic Properties of  $\beta$ -type Ti-Alloys Using Electronic Parameters, *Scr. Mater.*, 2006, **55**(5), p 477–480
18. Decker R F(1969) Strengthening Mechanisms in Nickel-Base Superalloys. Proc of Steel Strengthening Mech Symp, Zurich, Switzerland, May 5-6:1-24
19. D.C. Zhang, J.G. Lin, W.J. Jiang, M. Ma, and Z.G. Peng, Shape Memory and Superelastic Behavior of Ti-7.5Nb-4Mo-1Sn Alloy, *Mater. Des.*, 2011, **32**(8–9), p 4614–4617
20. S.J. Dai, Y. Wang, and F. Chen, Effects of Annealing on the Microstructures and Mechanical Properties of Biomedical Cold-Rolled Ti-Nb-Zr-Mo-Sn Alloy, *Mater. Charact.*, 2015, **104**, p 16–22
21. P.E.L. Moraes, R.J. Contieri, E.S.N. Lopes, A. Robin, and R. Caram, Effects of Sn Addition on the Microstructure, Mechanical Properties and Corrosion Behavior of Ti-Nb-Sn Alloys, *Mater. Charact.*, 2014, **96**(3), p 273–281
22. S. Guo, J. Zhang, X. Cheng, and X. Zhao, A Metastable  $\beta$ -Type Ti-Nb Binary Alloy with Low Modulus and High Strength, *J. Alloy. Compd.*, 2015, **644**, p 411–415
23. Q.K. Meng, S. Guo, Q. Liu, L. Hu, and X. Zhao, A  $\beta$ -Type TiNbZr Alloy with Low Modulus and High Strength for Biomedical Applications, *Prog. Nat. Sci. Mater. Int.*, 2014, **24**(2), p 157–162
24. X.H. Cao, X.L. Cao, and Q. Zhang, Nanoscale Indentation Behavior of Pseudo-Elastic Ti-Ni Thin Films, *J. Alloy. Compd.*, 2008, **465**(1–2), p 491–496
25. K. Gall, K. Juntunen, H.J. Maier, H. Sehitoglu, and Y.I. Chumlyakov, Instrumented Micro-Indentation of NiTi Shape-Memory Alloys, *Acta Mater.*, 2001, **49**(16), p 3205–3217
26. R. Liu, D.Y. Li, Y.S. Xie, R. Llewellyn, and H.M. Hawthorne, Indentation Behavior of Pseudoelastic TiNi Alloy, *Scripta Mater.*, 1999, **41**(7), p 691–696
27. W. Ni, Y.T. Cheng, and D.S. Grummon, Microscopic Superelastic Behavior of a Nickel-Titanium Alloy Under Complex Loading Conditions, *Appl. Phys. Lett.*, 2003, **82**(17), p 2811–2813
28. M. Tane, T. Nakano, S. Kuramoto, M. Hara, and M. Niinomi, Low Young's Modulus in Ti-Nb-Ta-Zr-O Alloys: Cold Working and Oxygen Effects, *Acta Mater.*, 2011, **59**(18), p 6975–6988
29. L. Zhang and H. Attar, Selective Laser Melting of Titanium Alloys and Titanium Matrix Composites for Biomedical Applications: A Review, *Adv. Eng. Mater.*, 2016, **18**(4), p 463–475